Chemical Engineering Journal 422 (2021) 130047

Contents lists available at ScienceDirect

Chemical Engineering Journal

journal homepage: www.elsevier.com/locate/cej

Dual-role of ZnO as a templating and activating agent to derive porous carbon from polyvinylidene chloride (PVDC) resin

Beodl Hwang [a], Seong-Hoon Yi [a], Sang-Eun Chun [a,b,*]

[a] School of Materials Science and Engineering, Kyungpook National University, 80 Daehak-ro, Buk-gu, Daegu 41566, Republic of Korea
[b] School of Industrial Technology Advances, Kyungpook National University, 80 Daehak-ro, Buk-gu, Daegu 41566, Republic of Korea

ARTICLE INFO

Keywords:
Activated carbon
Chemical activation
Templating
Polyvinylidene chloride (PVDC) resin
ZnO
$ZnCl_2$

ABSTRACT

Activated carbon, with its porous morphology and extremely high surface area, maintains the exclusive position as an electrode material in supercapacitors owing to its low manufacturing cost. Although its surface area can be boosted using a chemical etchant to create nanoscale pores, the use of chemicals requires a post-washing of the material to eliminate impurities. Herein, the activation of polyvinylidene chloride (PVDC) resin using ZnO chemical is described to prepare porous activated carbon materials for use as supercapacitor electrodes. During heat-treatment of a 1:1 mass ratio of PVDC resin:ZnO at 950 °C, activation and templating processes consecutively take place to produce porous carbon. Between 140 °C and 600 °C, $ZnCl_2$ formed from the conversion of ZnO chemically activates the carbon with creating micropores. Above 800 °C, unreacted ZnO from the initial activation is reduced to Zn upon oxidation of the carbon with the additional micropore creation. Above 907 °C the Zn evaporates to leave activated carbon with no impurities. Through this process, the sites initially occupied by ZnO would turn to the pores by templating. With a rationally-designed ZnO ratio, porous carbon can be produced without washing. The activated carbon exhibits a high quinone content that reacts with H^+ ions, with a high specific capacitance of 219 F g^{-1} in 1 M H_2SO_4 based on pseudocapacitance. However, the rate performance of this material is 55% due to the slow kinetics of the charge transfer reaction. On the contrary, a high quaternary-N content increases the rate capability of the material in 6 M KOH, where the double-layer mostly contributes toward charge storage.

1. Introduction

Owing to its porous structure, activated carbon has excellent sorption ability to store/separate a wide range of ions or particles; thus, is thus commonly used in various purification and storage applications [1–6]. As a result of it being a good conducting material with excellent absorption properties, activated carbon is mostly used as an electrode material in supercapacitors. It is synthesized via an organic precursor with the aid of a suitable transformation agent at an elevated temperature. Thermal processing of the precursor results in carbon being produced in the form of hexagonal graphene, and then a physical or chemical agent is used to create nanoscopic pores in the stacked graphene layers [7–9]. Two types of activation of the composed graphene layers can be achieved based on the agent employed in this process; physical or chemical activation [10–12]. Of the two activation routes, the physical process has been actively utilized to make activated carbon at a low cost because the process involves only a simple processing stage and low-priced H_2O or CO_2 reagents [1,13]. Although the physical method has superior economic advantages over its chemical counterpart, chemical activation has also been focused on based on it being used to develop small-sized pores in a material and, accordingly, a high specific surface area [14,15]. Furthermore, functional groups can be introduced to porous carbon materials via chemical reactions [16–19]. However, processes such as chemical etching require complicated processing stages involving mixing, impregnation, pyrolysis, and washing. Commonly, post-washing of a material with an acid is required to remove any heteroatoms related to the chemical agent. The laborious and tricky multi-stages of chemical processes are a significant hurdle in their scale up to the industrial synthesis of porous carbon. Thus, reducing the number of stages in porous carbon manufacture has long been desired for reducing the cost of microporous carbon with large surface area. In this regard, the aim is to devise a straightforward chemical activation route that does not require a post-washing stage. With a rational selection of raw material and chemical agent, this

* Corresponding author.
E-mail address: sangeun@knu.ac.kr (S.-E. Chun).

https://doi.org/10.1016/j.cej.2021.130047
Received 20 January 2021; Received in revised form 16 April 2021; Accepted 21 April 2021
Available online 27 April 2021

objective has been approached and is described herein.

Chemical activation typically follows the impregnation of a material with an etching agent and its subsequent pyrolysis at an elevated temperature [1,20]. To homogeneously etch the entirety of a raw material, the etching agent is initially dissolved in a solvent, and then the mixed solution is pyrolyzed to activate the material. When mixed with an etchant, a typical raw material requires more chemical agent content to develop high porosity [21]. This extra use of expensive chemical agents increases the production costs of the final carbon [22]. Moreover, carbon materials derived from chemical routes often contain various hetero-compounds that originate from the chemical used in the etching process [23–25]. The impurities from the chemical agent must be thoroughly removed from the final carbon product so that it can be used as a supercapacitor electrode in stable cycling [8]. Thus, the chemical activation needs to employ a reduced amount of chemicals to achieve low-cost etching and obtain pure final carbon. To maintain numerous pores, the chemical activation process should be designed to produce a porous material at low production costs, which might not be achieved by naively lowering the etchant amount. A highly porous structure can be achieved by using more chemicals, but low cost is associated with the minimal use of etching chemicals in a process. These two objectives are in direct conflict with one another, and thus there needs to be a compromise in the amount of chemicals used to achieve a material with a highly porous structure [26–28].

To achieve a high porosity carbon structure through the minimal usage of a chemical agent, the raw material that can be transformed into highly porous carbon during pyrolysis should be selected. A typical organic material used as a raw material for activation was not transformed into carbon with a high surface via a simple pyrolysis step without being activated. Several polymer materials have been carbonized via pyrolysis to achieve structures with the nano-scaled pores [29–31]. In this way, high surface area structures can be easily developed based on micropore formation from these polymer materials [32–34]. Polyvinylidene chloride (PVDC) can be pyrolyzed into carbon that has a high surface area of over 800 $m^2\ g^{-1}$ with micropore formation associated with the release of HCl gas [35–41]. Furthermore, PVDC resin produced from the polymerization of a vinylidene chloride monomer with other monomers is lower in cost to produce but has a similar chemical structure to that of pure PVDC. PVDC resin would therefore be a good raw material to activate and produce a porous carbon structure based on it being lower in cost than pure PVDC precursor. Considering the cost, the polyvinylidene chloride (PVDC) precursor is not as sustainable as the starting materials for industrial activated carbon, including coconut, coal, and wood, for industrial activated carbon. Nonetheless, the synthesis of porous carbon from PVDC resin is worthwhile studying to improve the conventional performance of supercapacitors by employing newly-processed carbon material for electrodes. The distinct and engineered properties of such electrode materials could enable us to overcome the standstill current performance of supercapacitors.

ZnO has commonly been used as a template to form materials that have large-sized pores [42,43]. Even though nanosized ZnO can be used to produce materials that have smaller pores because of its nanoscale dimensions, the use of nanosized ZnO should be avoided to keep manufacturing costs low [44,45]. The HCl gas released from PVDC resin during pyrolysis reacts with HCl to form $ZnCl_2$, which is a chemical agent widely used to form porous structures [46,47]. Therefore, the treatment of PVDC resin with ZnO would enable porous carbon materials to be produced with a wide pore size range based on ZnO templating and $ZnCl_2$ activation. Moreover, the ZnO would oxidize the preformed carbon at temperature above 800 °C, creating pores, and the reduced Zn would evaporate above 907 °C. Therefore, when a carbon precursor blended with appropriate ZnO content is pyrolyzed, the ZnO creates pores in its structure and can then be reduced and evaporated off at an elevated temperature. Thus, the use of ZnO in pore formation does not leave behind any chemical impurities, meaning that a post-washing process is not required after the activation of the structure in question. Although the alkaline hydroxides have been reported to be exceptionally effective in deriving the microporous morphology, ZnO is employed as a chemical etchant to thoroughly exploit the reaction process during the pyrolysis of PVDC. Chemical activation of a material also tends to affect the functional groups present in the final porous carbon structure produced [48]. Therefore, activated carbon prepared using ZnO would exhibit varying electrochemical performances in different pH solutions based on the functional groups present in its structure. Herein, a chemical route was designed and developed to enable porous carbon to be fabricated from PVDC resin based on the dual role of ZnO. Based on its evolved porous properties and functional groups, the electrochemical performance of the final activated carbon was explored in different pH electrolytes.

2. Experimental

2.1. Synthesis of the carbon

PVDC resin (F216, Asahi Kasei) was used as a raw material for the synthesis of the carbon material. Either ZnO (≥99.0% purity, Sigma Aldrich) or $ZnCl_2$ (98.0% purity, SAMCHUN) were used as a chemical activating agent for the generation of a porous carbon structure. The raw material and activation agent were mixed in weight ratios of 2:1 or 1:1 of PVDC resin (1 g) and ZnO or $ZnCl_2$ (0.5 or 1.0 g). A mixture with an appropriate ratio was mechanically mixed for 5 min in an agate mortar and pestle, and was then heated to 750 °C or 950 °C for 2 h at 5 °C min^{-1} under a flow of nitrogen gas (N_2) of 300 $cm^3\ min^{-1}$ in a horizontal tube furnace. In this process, the mixture was converted to carbon through pyrolysis, with no further washing of the material required after carbonization of the PVDC resin using the chemical agent. The carbon sample prepared from PVDC resin alone at 750 °C without the use of any chemical agent is referred to as P-750, designated as a control for comparison against the other samples prepared in this study. A sample processed using a chemical agent is denoted as P-*x*ZnO (or $ZnCl_2$)-*y* (*x*: weight of the chemical agent per 1 g of PVDC resin and *y*: the carbonization temperature) based on the mass ratio of the materials and temperature used in the synthesis.

2.2. Materials characterization

The thermogravimetric behavior of the materials was analyzed at a range of temperatures up to 1000 °C at a heating rate of 5 °C min^{-1} under a N_2 atmosphere using a thermogravimetric analyzer (auto TGA-DSC, SDT 650, TA Instruments, USA). Elemental analysis of the prepared carbon materials was conducted using energy-dispersive X-ray spectroscopy (EDS, X-max n80, Horiba, Japan). A field emission scanning electron microscope (FE-SEM, SU8220, Hitachi, Japan) was used to analyze the morphologies of the carbon materials. To measure the pore size distributions and specific surface areas of the materials, the adsorption/desorption of N_2 gas from the samples was monitored using an automated gas adsorption analyzer (Autosorb iQ, Anton Paar, Austria). N_2 adsorption/desorption was performed on the prepared carbon samples at 77 K after they had been degassed at 300 °C for 3 h to remove any adsorbed moisture and organic compounds from their structures. Their pore size distributions were measured using a quenched solid density functional theory model based on the measured adsorption and desorption isothermal curves. The specific surface areas of the samples were then calculated based on the Brunauer–Emmett–Teller (BET) method. The specific surface areas of the micropores in the samples were measured using the t-plot method. The total pore volumes of the samples were estimated from amount of N_2 adsorbed at a relative pressure of $P/P_0 = 0.99$. The crystal structures of the prepared carbon samples were measured using an X-ray diffractometer (XRD, EMPYREAN, Panalytical, UK) equipped with a Cu-Kα radiation source (λ = 1.5406 Å). The oxygen and nitrogen functional groups derived from the

PVDC resin were measured at a survey scan rate of 1 eV and a high-resolution scan rate of 0.1 eV using X-ray photoelectron spectroscopy (XPS, NEXSA, ThermoFisher, USA) with an Al-Kα radiation source (1486.6 eV). The high-resolution spectra of the samples were fitted using Gaussian (70%)–Lorentzian (30%) functions.

2.3. Electrochemical characterization

In the electrode assembly used in the electrochemical measurements, polytetrafluoroethylene (PTFE) (≥350 μm, Sigma Aldrich) and carbon black (Ketjenblack EC-600JD, Lion) were used as a binder and conductor, respectively. The synthesized carbon (active material) samples were mixed with binder and conductor in a mass ratio of 85% active material, 10% binder, and 5% conductor using an agate pestle and mortar. Then, around 3 mg of the resulting mixture was deposited on a mesh substrate using a hydraulic press under a pressure of 20 MPa.

Three electrolytes were employed, 0.5 M K_2SO_4 (99.0%, Alfa Aesar), 1 M H_2SO_4 (98%, DAEJUNG), and 6 M KOH (85%, Alfa Aesar), each with different acidities. The nickel or stainless-steel substrates were used to prevent any side reactions occurring depending on the chosen electrolyte. Nickel mesh (100 mesh) was used in K_2SO_4 and KOH solutions, and stainless-steel mesh (100 mesh) was used in H_2SO_4 solution. Reference electrodes of a saturated calomel electrode (SCE) in K_2SO_4 and H_2SO_4 electrolyte and mercury oxide (Hg/HgO) in KOH electrolyte were used. All measured potentials were converted to the normal hydrogen electrode scale using the following relationships, $E_{NHE} = E_{SCE} + 0.242$ V and $E_{NHE} = E_{Hg/HgO} + 0.098$ V. A platinum wire was used as a counter electrode. All electrochemical analyses were performed using a potentiostat (VMP3, Bio-logic, France). Electrochemical impedance spectroscopy measurements were carried out at a specific potential with an additional sine waveform with an amplitude of 5 mV in the frequency range of 0.1 Hz to 1000 kHz.

3. Results

3.1. Selection of the polymer precursor and chemical agent for the synthesis of highly porous carbon

An organic material is a typical raw material used to formulate porous carbon that has high specific surface areas with the help of a pore formation agent. Porous carbons with high surface areas are suitable candidates for use as electrodes in supercapacitors because their high surface areas allow more ion adsorption for double-layer charging [49,50]. PVDC has a carbon backbone structure with periodically dangling chlorine and hydrogen atoms. Both these elements of the PVDC can be transformed into HCl gas during the pyrolysis of the material, leaving a pore in an evacuated elemental site [35,41]. The pores created on its surface in this way have nanoscale dimensions, implying that the material has a high surface area. The surface area of the carbon derived from PVDC is 4–110 times higher than that derived from other raw materials via direct pyrolysis (Fig. 1(a)) [51–54]. The PVDC resin comprises mainly PVDC with additional oxygen and nitrogen, which possibly convert to oxygen- or nitrogen-containing functional groups in the carbon matrix upon thermal treatment (Fig. 1(b)) [55–57]. These functional groups are oxidized or reduced upon interacting with H^+ or OH^- ions in aqueous electrolyte [58,59]. This charge transfer reaction provides an additional faradaic reaction by which to store electrical charge. In this regard, the PVDC resin was selected as a starting material to derive a porous carbon material with functional groups.

The chemical reaction that occurs during the pyrolysis of the PVDC resin was analyzed by carrying out thermogravimetric analysis differential scanning calorimetry (TGA-DSC) measurements up to 900 °C. It was observed that the mass of the material rapidly decreases at around 200 °C with an exothermic peak, attributable to the HCl gas released from the decomposition of H and Cl [60] (Fig. 1(c)). At approximately 600 °C, there is a weak endothermic peak in the DSC data alongside a small reduction in the mass of the sample, as a result of the detachment of H from the formed carbon chain, forming a nanosized pore [36]. After pyrolysis up to 900 °C, a yield of 28% was attained, slightly higher than the theoretical maximum carbonization yield of 25%, which infers that the carbon in the PVDC and other elements in the resin still sustained after the pyrolysis.

3.2. Design of the activation and templating process using ZnO

Direct pyrolysis of the PVDC resin led to the formation of microporous carbon with a relatively low surface area of 887 $m^2\ g^{-1}$ for use as a supercapacitor electrode, even though PVDC resin developed the high specific surface area compared to other organic raw materials. The increment in the surface area was pursued by multiple pore formation reactions using the activating agent. In particular, an attempt was made to take advantage of the HCl gas emitted during the pyrolysis of the PVDC resin. As mentioned earlier in introduction, ZnO is commonly used as a template agent and reacts with HCl to produce $ZnCl_2$, which is a common chemical activating agent used to create pores in carbon materials [61,62]. ZnO can also be used to activate carbon above 800 °C, and is then reduced to Zn residue, which can be evaporated off above 907 °C. Therefore, if the ZnO content was rationally regulated in the initial mixture, the PVDC resin can be transformed into a porous carbon material without any Zn-related products remaining in the structure. The formation of a pure porous carbon material in this way would not require any laborious or tedious washing processes to be carried out after the activation process, which are currently considered as hurdles in the scale up of the chemical activation process [63].

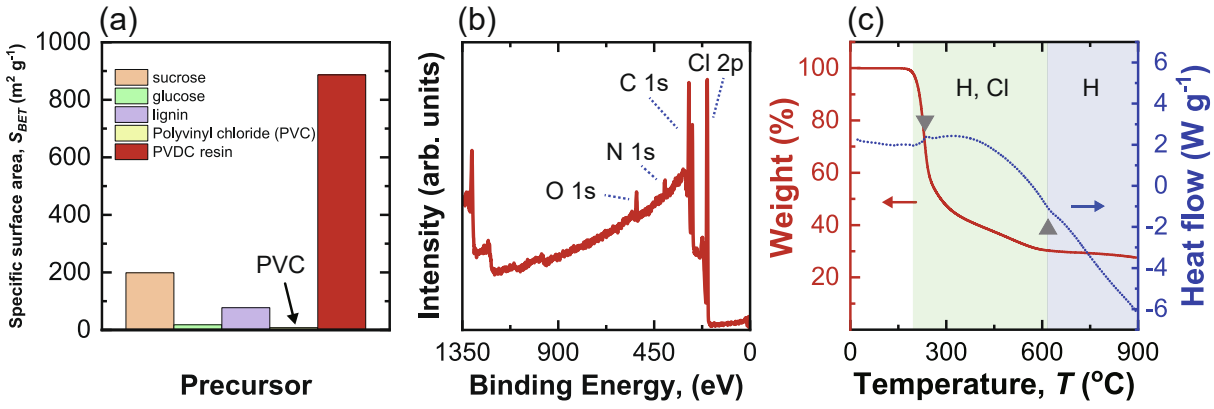

Fig. 1. (a) Specific surface area of the carbon materials obtained from the pyrolysis of various organic precursors, (b) XPS survey spectrum of the PVDC resin, and (c) TGA-DSC results of the PVDC resin.

The role that ZnO plays during the thermal treatment was investigated by pyrolyzing two samples that have different ZnO contents, a mixture of PVDC resin and ZnO in mass ratios of 1:0.5 (P-0.5ZnO-950), and 1:1 (P-1ZnO-950), with the results shown in Fig. 2(a). Given the TGA-DSC analysis of the PVDC resin and ZnO mixtures, the chemical reactions that occur during pyrolysis were determined and are schematically shown in Fig. 2(b). Compared to the initial change in mass that occurs at 200 °C for the PVDC resin alone, a significant mass reduction occurs for both of the PVDC resin and ZnO mixtures at a lower temperature of 140 °C. The HCl gas released from these samples then reacts with ZnO based on the following chemical reaction [64]:

$ZnO + 2HCl \rightarrow ZnCl_2 + H_2O$ (1)

Since the ZnO accelerates the detachment of the chlorine, the mass reduction is observed at a lower temperature of 140 than 200 °C [65]. $ZnCl_2$ induces a porous structure in the carbon based on its etching effect between 140 °C and 600 °C, a process designated as the first activation. The transformation of ZnO to $ZnCl_2$ was confirmed based on the pyrolysis of the PVDC resin and ZnO mixture in a mass ratio of 1:0.5 at 400 °C, in which the generated $ZnCl_2$ cannot be removed. The EDS measurements of the mixture pyrolyzed at 400 °C show the presence of Zn, Cl, and O in the sample. In the EDS mapping image of Fig. 2(c), the Cl element appears among the Zn element. Moreover, the atomic ratio of Zn:Cl was close to 1:2, indicating that $ZnCl_2$ was formed. The O present in the EDS mapping image shows the presen ce of unconverted ZnO in the sample. The $ZnCl_2$ that originates from the ZnO at above 140 °C mostly creates micropores in the sample [61,66]. Between 400 °C and 600 °C, a second significant mass change was observed corresponding to the evaporation of $ZnCl_2$ [64].

Another rapid reduction in mass occurs at above 800 °C, ascribed to a reduction in residual ZnO that was not previously transformed into $ZnCl_2$ below 600 °C [67–69]:

$ZnO + C \rightarrow Zn + CO$ (2)

The oxidation of carbon by the residual ZnO above 800 °C is designated as the second activation, leaving the micro-sized pores. The reduced Zn then evaporates off at above 907 °C, leaving meso-sized pores in the carbon [69]. If the amount of HCl gas released from the PVDC resin is sufficient, it can react with all ZnO in the mixture. The ZnO is then fully transformed to $ZnCl_2$ at 800 °C. One mole of PVDC releases 2 mol of HCl gas, which later reacts with 1 mol of ZnO as shown in Reaction (1). The HCl gas released from 1 g of PVDC resin (0.0103 mol) converts 0.84 g of ZnO (0.0103 mol) into $ZnCl_2$ during the first activation. Thus, when PVDC resin and ZnO are mixed at a mass ratio of 1.0:0.5, all of the ZnO should be consumed in the first activation (P-0.5ZnO-950). In contrast, during the pyrolysis of mixed PVDC resin and ZnO at a mass ratio of 1.0:1.0, some ZnO remains after the first activation, which subsequently participates in the second activation (P-1ZnO-950). Comparing the two samples after the second activation at above 800 °C, the mass reduction was more considerable in the P-1ZnO-950 sample than in the P-0.5ZnO-950. During pyrolysis up to 950 °C, the initial ZnO additive was converted to $ZnCl_2$ and Zn at 140 °C and 800 °C, respectively. The sites preoccupied by ZnO remained in the structure as large-sized mesopores and macropores through the templating process [70].

The yield of the carbon produced was calculated for all of the prepared samples based on the final mass versus the initial precursor mass to estimate the conversion efficiency of the raw material (Table 1). The chemical role of ZnO at a specific temperature was investigated in activation experiments with $ZnCl_2$ and ZnO at 750 °C or 950 °C. The yield of the P-0.5$ZnCl_2$-750 sample was 29%, marginally lower than that of the P-750 sample (yield = 30%). The activation of the sample by $ZnCl_2$ obtained a very high yield of the final product, as previously reported in other studies [71,72]. The yield of the P-0.5ZnO-750 sample was similar (28%). The chemical activation by $ZnCl_2$ during the preparation of P-0.5$ZnCl_2$-750 probably also occurred during the pyrolysis of the 0.5ZnO-750 sample. In this activation process, the sites occupied by the converted ZnO acted as a template, leaving large-sized pores in the final product. In the proposed process, the additional templating was presumed to slightly decrease the carbon production yield to 28%. Comparing the P-0.5ZnO-750 and P-0.5ZnO-950 samples, raising the temperature from 750 °C to 950 °C reduced the production yield from 28% to 26%. This yield drop might be attributable to second activation by the ZnO agent. When 0.5 g of ZnO was used with 1.0 g of PVDC resin, the second activation by ZnO was not expected because the ZnO should have been fully converted to $ZnCl_2$ between 140 °C and 600 °C. Nonetheless, the TGA–DSC curves show that a part of the ZnO remained after the first activation temperature, which entered the second activation; accordingly, the mass reduced between 800 °C and 907 °C (see Fig. 2 (a)). Moreover, the lower yield in P-1ZnO-950 (23%) than in P-0.5ZnO-950 (26%) in Table 1 indicates that the second activation predominantly occurred at approximately 800 °C (see also the TGA–DSC profiles in Fig. 2(a)). After two consecutive activations and templating occurred during pyrolysis of the PVDC resin:ZnO (mass ratio 1.0:1.0), the yield of

Table 1
Final yields of samples prepared under varying conditions.

Sample	P-750	P-0.5$ZnCl_2$-750	P-0.5ZnO-750	P-0.5ZnO-950	P-1ZnO-950
Yield (%)	30	29	28	26	23

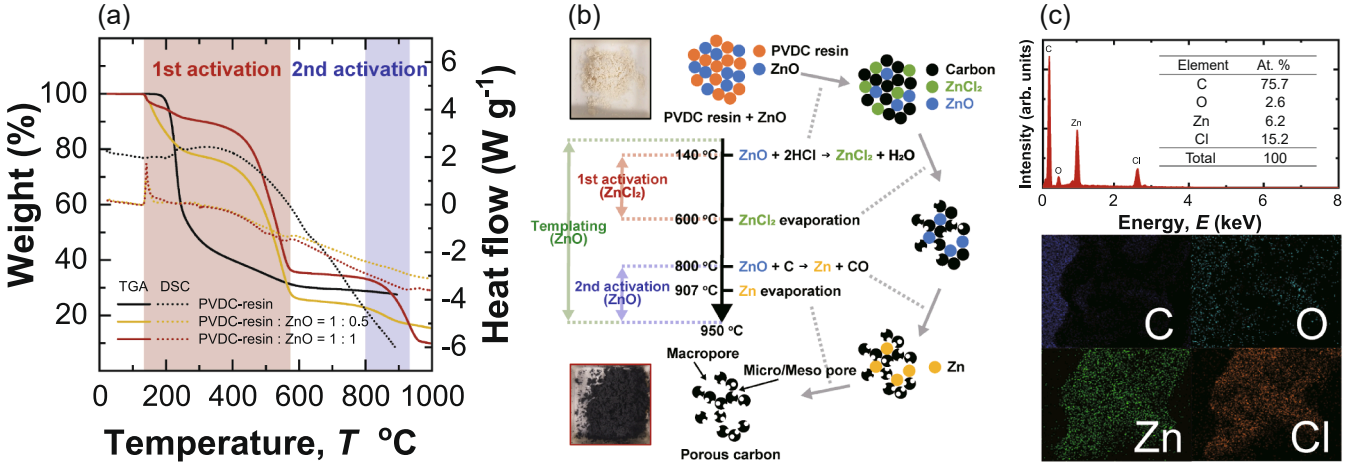

Fig. 2. (a) TGA-DSC profiles of the PVDC resin and its mixtures with ZnO, (b) scheme of the chemical process of the PVDC resin mixed with ZnO during the pyrolysis, and (c) EDS analysis of the mixture after pyrolyzed at 400 °C.

this process achieved 23%.

3.3. Physical and chemical analysis of the carbon samples treated using $ZnCl_2$ and ZnO

The surface morphologies and porous properties of the carbon samples produced via different routes were analyzed based on their SEM images (Fig. 3). The SEM image of the P-750 sample (Fig. 3(a)) reveals a polished surface that underwent the dichlorination process, and numerous micropores formed during pyrolysis. The P-0.5$ZnCl_2$-750 sample shown in Fig. 3(b) has a swollen texture due to it being activated by $ZnCl_2$, which is a well-known foaming agent. This sample does not appear to be porous from its SEM image, inferring that only small-sized pores are created via $ZnCl_2$ activation [73]. In contrast, the P-0.5ZnO-750 sample shown in Fig. 3(c) has a porous morphology, due to both $ZnCl_2$ activation and ZnO templating occurring in this sample, with the larger pores in this sample attributed to the templating effect. Meanwhile, numerous pores are present on the surface of the P-1ZnO-950 sample shown in Fig. 3(e), when viewed at a high magnification these were observed to be various sizes of pores. When PVDC resin and ZnO are reacted in a mass ratio of 1:1, not all of the ZnO reacts with the PVDC resin and is transformed into $ZnCl_2$ between 140 °C and 600 °C. Accordingly, any residual ZnO that remains unreacted during the first activation oxidizes the carbon above 800 °C and forms the pores. Besides this, the reduced Zn that is formed from ZnO evaporates, leaving behind a pore as a result of a templating effect. In contrast, as shown in Fig. 3(d), the P-0.5ZnO-950 sample does not exhibit the fine macro-sized pores at high magnification, inferring that the second activation process does not affect the evolution of the pores in this employed mass ratio.

The morphologies of the samples shown in the SEM images were quantitatively examined by recording the N_2 adsorption/desorption profiles and pore size distributions of the materials, as shown in Fig. 4 (a–b). Compared to the P-750 sample, all the other carbon samples treated using ZnO or $ZnCl_2$ exhibit isotherms showing that a high amount of N_2 is adsorbed on these samples at a P/P_0 of 0.1, implying that they have enhanced micropore contents (Fig. 4(a)) [75]. Compared to P-750, the pore distribution of the sample treated with $ZnCl_2$, P-0.5$ZnCl_2$-750, clearly shows that the number of micropores with sizes between 1.2 and 2 nm was considerably increased (Fig. 4(b)). However, no enhancement was observed in the meso-sized range when $ZnCl_2$ activation was used, inferring that$ZnCl_2$ does not seem to produce meso-sized pores. When ZnO replaced $ZnCl_2$ agent in the activation of PVDC resin, the number of micropores with 1.2 nm in size decreased in the P-0.5ZnO-750 sample, but the porosity was enhanced in all other ranges. This result indicates that the use of ZnO leads to larger sized pores being developed than when $ZnCl_2$ is used. As a result, it can be seen that ZnO is more effective than $ZnCl_2$ in expanding the surface area of a sample based on its additional template effect compared to $ZnCl_2$ activation (Table 2). When the treatment temperature of the ZnO-activated samples was elevated from 750 °C to 950 °C (P-0.5ZnO-750 vs. P-0.5ZnO-950), the specific surface area of the sample reduced from that of the sample treated at a low temperature. It is thought that the higher temperature induces the graphitization of the composed graphene layers and seems to eliminate the small-sized pores in the sample, as shown in Fig. 4(b) [76].

Out of all of the samples, the largest surface area was achieved for the P-1ZnO-950 sample, which is assumed to undergo both the two activations and templating processes (Table 2). A comparison of the P-1ZnO-950 and P-0.5ZnO-950 samples reveals that the mostly micropores in these materials are enhanced by adding a higher amount of ZnO to the reaction mixture, see Fig. 3(b) and Table 2. The excess of ZnO that is not transformed to $ZnCl_2$ reacts with the carbon produced from the PVDC resin, leading to evolution of the primary micropores in the structure. Overall, the second activation by ZnO seems to mainly contribute toward the formation of micropores. The treatment of the PVDC resin in a 1:1 mass ratio with ZnO at 950 °C greatly enhances the specific surface area of the material in terms of both its microporosity and mesoporosity based on both activation and templating processes being promoted by the ZnO. A key advantage of this process is that no by-product is produced, even elemental Zn. Compared to the results in relevant previous studies, a higher surface area carbon material was produced in this work using a lower chemical agent to raw material ratio (Table 3). Consequently, no additional post-treatment, including washing, is required in the route proposed in this work.

The structural changes that take place in the samples prepared using the different chemical processes were analyzed using X-ray diffraction and Raman spectroscopy. All of the prepared carbon samples featured hexagonally structured graphene stacking layers with low crystallinity, as evidenced by the broad peaks of (002), (100), and (110) in their powder X-ray patterns (Fig. 5(a)). The broad D-(1350 cm^{-1}) and G-bands (1600 cm^{-1}) in the Raman spectra further reveal that the prepared carbon samples exhibit turbostratic disorder (Fig. 5(b)) [87]. The extent of the parallel stacking in the graphene layers was estimated based on the empirical R value, measured from the (002) Bragg peak versus the background peak (Table 4) [71,88,89]. Compared to the P-750 sample, P-0.5$ZnCl_2$-750 contains numerous micropores due to the effect of the activation of the sample, but they both have similar R values. The similar R values of the samples indicates that $ZnCl_2$ does not forcefully break the stacking of the layers based on the aromatization by $ZnCl_2$ [90,91]. The P-0.5$ZnCl_2$-750 sample shows a lower I_D/I_G value

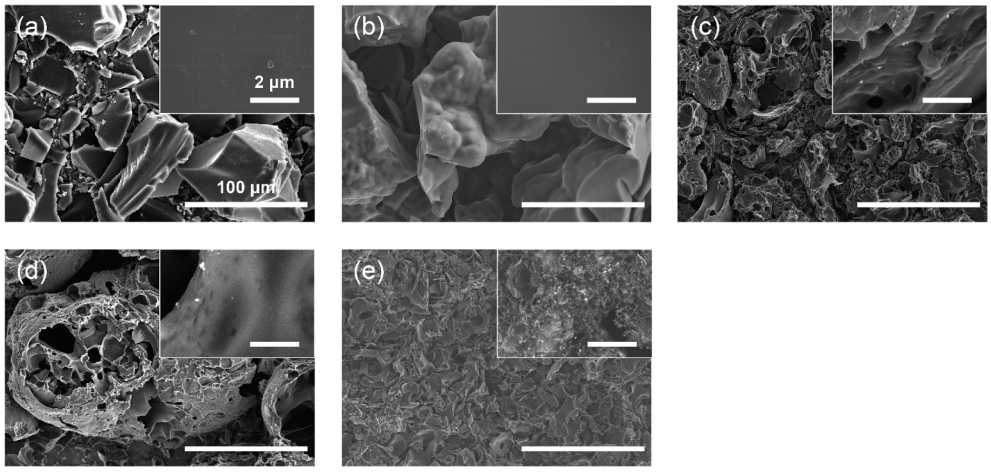

Fig. 3. SEM micrographs of (a) P-750, (b) P-0.5$ZnCl_2$-750, (c) P-0.5ZnO-750, (d) P-0.5ZnO-950, and (e) P-1ZnO-950 at 10000 × . Scale bars: 100 μm (inset: 500× magnification, scale bars: 2 μm).

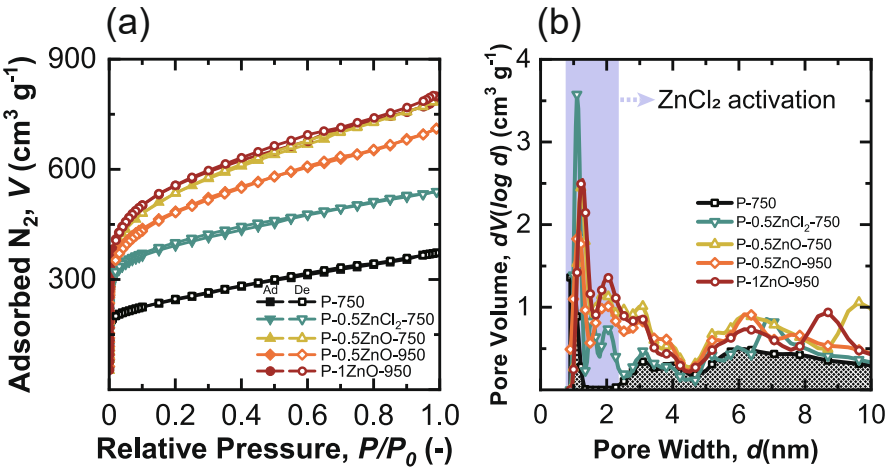

Fig. 4. (a) N_2 adsorption/desorption isotherms and (b) pore size distributions for all samples.

Table 2
Comparison of the porous properties of the obtained carbon samples in terms of their specific BET surface areas, the surface areas corresponding to micropores and external pores, and their total pore volumes.

Sample	S_{BET} [a] ($m^2\ g^{-1}$)	S_{micro} [b] ($m^2\ g^{-1}$)	$S_{external}$ [b] ($m^2\ g^{-1}$)	V_{total} [c] ($cm^3\ g^{-1}$)
P-750	887	493	395	0.58
P-0.5ZnCl$_2$-750	1462	1009	454	0.83
P-0.5ZnO-750	1927	1153	775	1.24
P-0.5ZnO-950	1785	1043	701	1.10
P-1ZnO-950	2005	1301	704	1.14

[a] Calculated using a multi-point BET method
[b] and [c] determined using the t-plot method[74]
[c] Estimated at $P/P_0 = 0.99$

Table 3
Comparison of the activation conditions adopted in this study with those employed in previous studies.

Activation agent	Activating agent/ precursor	Pyrolysis temperature (°C)	Specific surface area ($m^2\ g^{-1}$)	Reference
ZnO	1	950	2,005	This work
KOH	1.5	600	1,342	[51]
KOH	2	840	1,626	[77]
KOH	3	800	1,568	[78]
KOH	4	800	3,173	[79]
KOH	5	700	1,977	[80]
H_3PO_4	1	800	763	[81]
H_3PO_4	4	800	1,481	[82]
H_3PO_4	5	600	2,955	[83]
$ZnCl_2$	2	700	1,155	[84]
$ZnCl_2$	4	850	1,565	[85]
$ZnCl_2$	4	600	2,080	[86]

than the P-750 sample, with the lower intensity ratio of the D- to G-bands inferring lower disorder of the carbon structure (Table 4) [92]. The functional group removal by $ZnCl_2$ appeared to reduce the number of defects [93]. The treatment of the samples with ZnO instead of $ZnCl_2$ led to them having decreased R values, showing the effective scattering of the graphene layers by ZnO. Specifically, the P-1ZnO-950 sample has the lowest R value among all of the treated samples, with the highest I_D/I_G value, inferring that a large number of defects are formed in this sample as a result of both activation and templating effects.

3.4. Electrochemical behavior of the fabricated carbon samples as supercapacitor electrodes

The electrochemical behavior based on the electric double-layer charging of the evolved porous structure was analyzed using cyclic voltammetry (CV) in neutral K_2SO_4 solution (Fig. 6(a)). The measured specific capacitances were tabulated in Table 5. The P-750 sample that features mainly micropores exhibits a minimal current over a positive potential range based on the limited interaction that can take place between the narrow pores in the structure of the electrode and the large SO_4^{2-} ions of the electrolyte. The other carbon electrodes treated using $ZnCl_2$ and ZnO exhibit rectangular-shaped CVs based on their enlarged pore structures, inferring that the large SO_4^{2-} ions of the electrolyte have free access to the developed pores. The P-1ZnO-950 sample with the largest specific surface area of 2005 m g^{-1} showed the highest specific capacitance of 102 F g^{-1} (Table 5). The effect of the porous structure on the electrochemical performances of the electrodes was inferred from the impedance spectra. All Nyquist plots displayed the typical behavior of a double-layer capacitor, i.e., an initial semicircle at high frequencies and a consecutive sloped line. The impedance spectrum of P-1ZnO-950 in Fig. 6(b) exhibits a smaller semicircle in high-frequency ranges compared to that of P-0.5ZnO-950, inferring lower inhibition to ionic transfer. Moreover, the line at low frequencies is close to vertical capacitive behavior, referring the facile access of the electrolyte ion onto an electrode [94,95]. Looking at these results, it appears that the second activation process effectively increases the average pore size. This enlarged pore size is also reflected in the higher rate retention of P-1ZnO-950 of 61% versus 27% for the P-750 sample (Fig. 6(c)). The second activation process effectively allows the assembled activated carbon to perform as an electrode for supercapacitors, with excellent rate capability.

3.5. Electrochemical performance in electrolytes of different pH values

The surface functional groups present on the carbon can contribute toward the additional pseudocapacitive charge storage of the electrode based on oxidation/reduction processes other than double-layer capacitance. XPS measurements were performed on all of the carbon samples to investigate the evolution of the functional groups during the different synthetic routes, as shown in Fig. 7(a–b). Peaks related to oxygen-containing groups can be observed in the high-resolution O 1s spectra shown in Fig. 7(a) at 531.5, 532.5, 533.5, and 535 eV, which can be attributed as belonging to quinone (C=O, O-I), phenol (C–OH, O-II), and carboxylic acid (COOH, O-III) groups, and chemisorbed water (O-IV) [96,97], with the corresponding data shown in Table 6. Compared to the sample pyrolyzed directly from PVDC resin (P-750), all of the samples

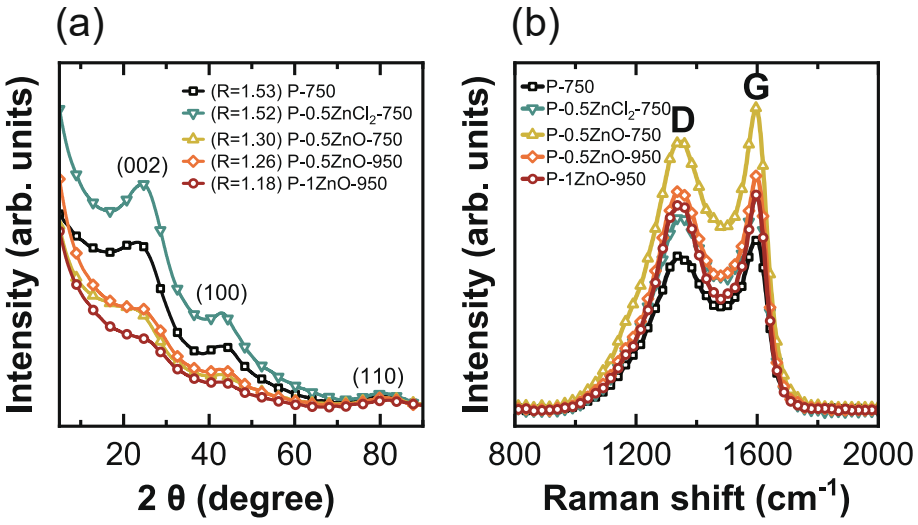

Fig. 5. (a) XRD patterns and (b) Raman spectra of all the prepared carbon samples.

Table 4
Estimated empirical R and I_D/I_G values.

Sample	R value	I_D/I_G
P-750	1.53	0.92
P-0.5ZnCl$_2$-750	1.52	0.90
P-0.5ZnO-750	1.30	0.93
P-0.5ZnO-950	1.26	0.93
P-1ZnO-950	1.18	0.96

treated using ZnO or $ZnCl_2$ exhibit increased quinone content and reduced carboxylic acid content. $ZnCl_2$ dehydrates the raw material, and accordingly, the carboxylic acid groups that form hydrogen bonds are reduced. Instead, there was an increase in quinone groups doubly-bonded to oxygen. Compared to treatment of the samples at 750 °C, an elevated temperature of 950 °C decreases the number of functional groups present in the samples, thus lowering their pseudocapacitance based on a reduced redox process (Table 6) [98,99]. Specifically, high heat-treatment at 950 °C largely reduces the fraction of carboxylic acids present in the samples (Table 6), as this temperature is sufficient enough to remove unstable carboxylic acid groups due to their weak bonding to hydrogen [100,101]. The reduced number of carboxylic acid groups interacting with OH– would decrease the pseudocapacitance effect of the sample in the alkaline electrolyte. In contrast, the quinone content that reacts with H^+ ions increased upon both ZnO and $ZnCl_2$ treatments, thus showing that all of the treatments of the samples would improve

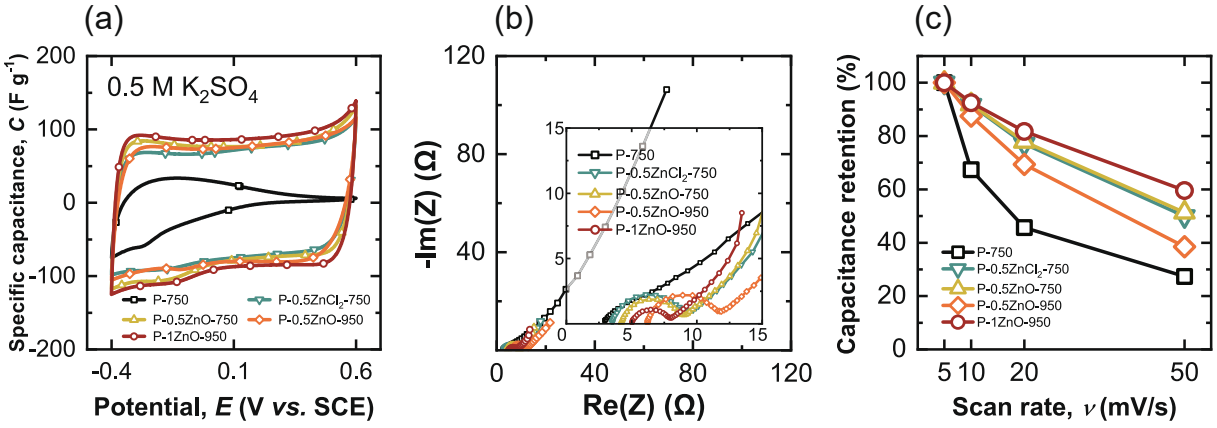

Fig. 6. (a) Cyclic voltammograms recorded at a scan rate of 5 mV s^{-1}, (b) impedance spectra, and (c) rate performances of all of the prepared carbon samples measured in neutral K_2SO_4 electrolyte.

Table 5
Specific capacitance and rate capability of the samples in different electrolytes.

Sample	K_2SO_4 Specific capacitance, C (F g^{-1})	Rate capability (%)	H_2SO_4 Specific capacitance, (F g^{-1})	Rate capability (%)	KOH Specific capacitance, C (F g^{-1})	Rate capability (%)
P-750	22	27	83	48	178	69
P-0.5ZnCl$_2$-750	82	51	187	49	168	72
P-0.5ZnO-750	94	51	207	44	201	69
P-0.5ZnO-950	89	38	173	58	156	67
P-1ZnO-950	102	61	219	55	201	79

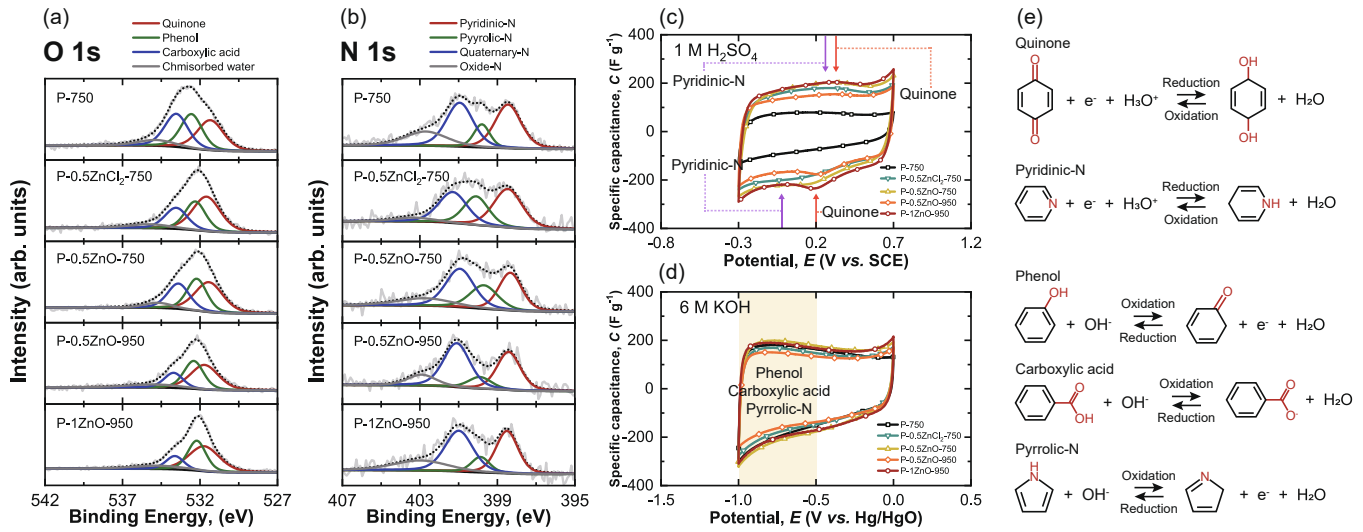

Fig. 7. High-resolution (a) O 1s and (b) N 1s XPS spectra and CVs of the prepared carbon samples in (c) 1 M H_2SO_4 and (d) 6 M KOH electrolyte. (e) Expected oxidation/reduction reactions of the evolved functional groups.

Table 6
XPS results of all of the prepared carbon samples.

Sample	Oxygen					Nitrogen				
	At. %	Quinone (O-I)	Phenol (O-II)	Carboxylic (O-III)	Water(O-IV)	At. %	Pyridinic-N (N-6)	Pyrrolic-N (N-5)	Quaternary-N (N-Q)	Oxide-N (N-X)
P-750	5.1	31.4	29.3	30.8	8.5	3.6	34.7	11.3	35.8	18.2
P-0.5ZnCl$_2$-750	4.3	43.5	27.1	21.8	7.6	2.8	38.7	24.8	31.1	5.3
P-0.5ZnO-750	6.9	38.4	29.4	25.6	6.6	3.5	28.8	21.7	36.0	13.5
P-0.5ZnO-950	3.2	40.6	32.8	16.9	9.7	2.5	33.9	10.2	44.1	11.8
P-1ZnO-950	4.3	44.2	31.7	13.9	10.2	1.9	32.2	9.8	39.3	18.7

their specific capacitance in acidic electrolyte. The nitrogen-containing functional groups that are present in the materials feature pyridinic-N (N-6), pyrrolic-N (N-5), quaternary-N (N-Q), and oxide-N (N-X), which show peaks at 398.3, 399.8, 401, and 403 eV, respectively, in the high-resolution N 1 s spectra shown in Fig. 7(b) [102].

Given the estimation of the functional groups in the prepared carbon samples, their pseudocapacitive behavior was investigated using CV involving assembled carbon electrodes in the acidic and alkaline electrolytes 1 M H_2SO_4 and 6 M KOH, respectively, as shown in Fig. 7(c) and (d). The sample treated using $ZnCl_2$ at 750 °C, P-0.5ZnCl$_2$-750, exhibits a reduction peak at 0 V in 1 M H_2SO_4 solution, where the redox peak at around 0 V can be attributed to pyridinic-N group (Fig. 7(e) and Table 6) [103]. Meanwhile, the samples prepared using ZnO at 750 °C and 950 °C show reduction peaks in their CVs at about 0.1 and 0.2 V, respectively. As seen in their XPS spectra, all of the prepared carbon samples show increased quinone group content, which is oxidized/reduced at around 0.2 V [103]. The redox behavior of the quinone group enhanced the specific capacitance of the prepared carbon samples when used as electrodes (Table 5). The sample prepared using 1 g of ZnO at 950 °C, P-1ZnO-950, exhibits the highest specific capacitance of 219 F g^{-1} among all of the samples, which can be ascribed the expansion of the porous structure that occurs as a result of the second activation process and the presence of quinone functional groups in this material. Furthermore, in KOH solution, asymmetric CVs were recorded based on the redox reaction of phenol, carboxylic acid, and pyrrolic-N over a negative potential range, with no prominent redox peaks observed, as shown in Fig. 7(d) [104]. Comparing the CVs of the samples prepared using different treatments, no significant differences were observed. Even though a large improvement in the surface areas of the samples were achieved after their treatments, their capacitance did not correspondingly improve, which may be due to the reduction of the carboxylic acid groups after treatment using $ZnCl_2$ or ZnO, as shown in the XPS analysis (Table 6).

In terms of the actual merits of the supercapacitors, their rate performances were measured in various electrolytes, with the results shown in Fig. 8(a) and (d). The rate capabilities of the samples were analyzed according to the estimated impedance properties of the assembled electrodes, as shown in Fig. 8(b) and (e). The carbon prepared with 1 g of ZnO at 950 °C (P-1ZnO-950) achieved the higher rate performances than other samples in both H_2SO_4 and KOH solutions. The open porous structure evolved from the activations and templating enabled the facile transport of electrolyte ions during the charging process. The rate performance of the P-1ZnO-950 sample was higher in KOH solution than in H_2SO_4 solution (79% vs. 55%). This result can be attributed to the larger contribution of double-layer capacitance than pseudocapacitance to the charge storage in KOH solution [59,105,106]. Moreover, the rate performances were higher in the H_2SO_4 and KOH solutions than in K_2SO_4 solution owing to the larger conductivities of the former solutions. Moreover, the rate performances of all carbon electrodes were higher in KOH solution than in H_2SO_4 solution: in KOH solution, all carbon electrodes presented weak interfacial resistances in the range of 0.7–1.7 Ω (Fig. 8(e)). This is as a result of the ions in the KOH electrolyte being smaller than those in the neutral or acidic electrolyte meaning that the porous morphologies of the prepared carbon materials do not limit the adsorption of the conducting ions in KOH. Therefore, excellent rate performances were achieved in the CVs of the carbon samples recorded in KOH solution. Specifically, P-1ZnO-950 exhibits the best rate performance of 79%.

4. Conclusion

A straightforward chemical method was designed to form porous

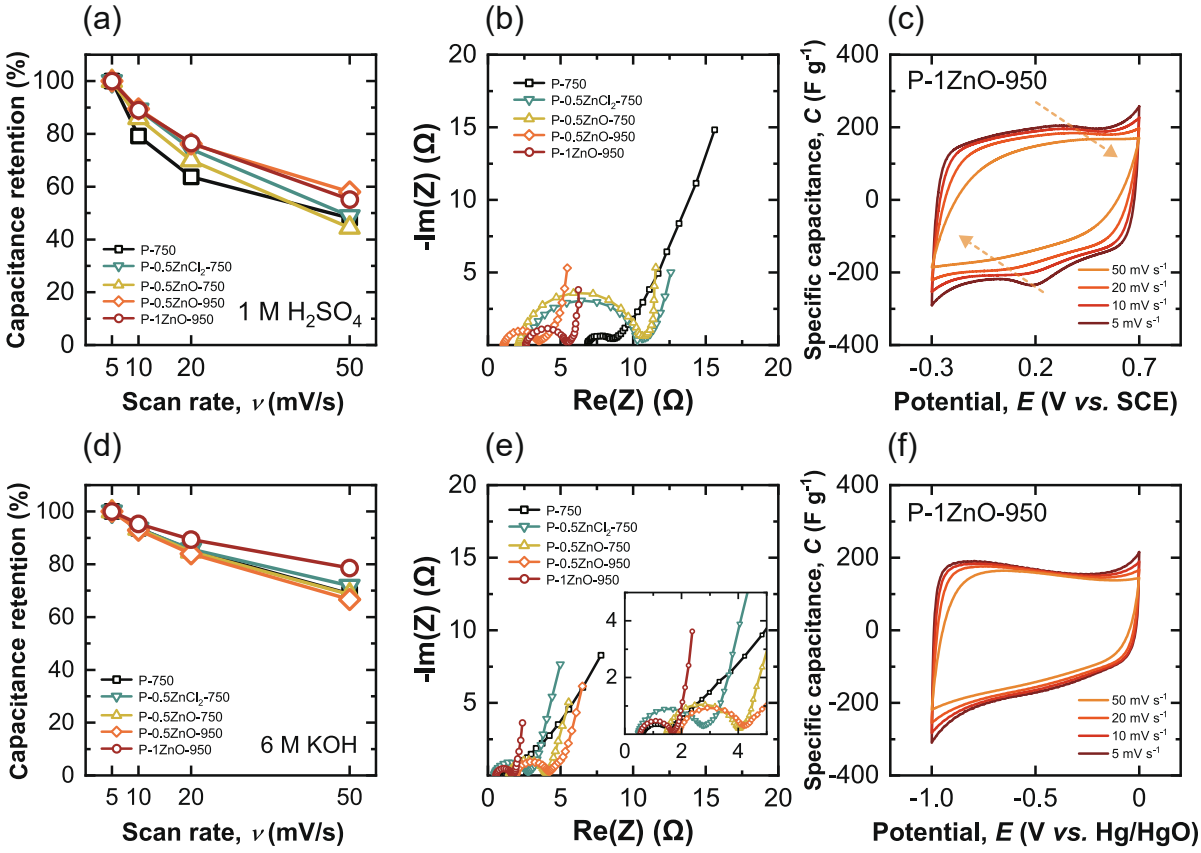

Fig. 8. (a) Rate capabilities, (b) impedance spectra, and (c) specific capacitances of carbon samples recorded in 1 M H_2SO_4 acidic electrolyte; (d) rate capabilities, (e) impedance spectra, and (f) specific capacitances measured in 6 M KOH alkaline electrolyte.

activated carbon for an electrode in aqueous supercapacitors using PVDC resin treated with ZnO, which plays a dual role in the chemical activation and templating. When PVDC resin and ZnO in a mass ratio of 1:1 are pyrolyzed at 950 °C, PVDC resin is turned into highly microporous carbon by H and Cl decomposition, yielding HCl gas which combines with ZnO and then forms $ZnCl_2$. The $ZnCl_2$ chemically etches the derived carbon between 140 °C and 600 °C, creating the micropores. Any unreacted ZnO left over from the first activation oxidizes the preformed carbon above 800 °C with creating mostly microsized pores while being reduced to Zn, which evaporates off at around 907 °C. Through the whole process, the occupied ZnO sites take part in templating the carbon by transforming and escaping ZnO.

The porous carbon prepared via the combination of the activations and templating by ZnO at 950 °C, P-1ZnO-950 samples, exhibits a high yield of 23% and an enormous surface area of 2005 $m^2\,g^{-1}$, which contains both micropores and mesopores. In a neutral K_2SO_4 solution, a high specific capacitance of 102 F g^{-1} was achieved based on the high specific surface area, and a high rate capability of 61% compared to 27% of the customarily pyrolyzed carbon was obtained by the expanded pore diameter. Furthermore, this porous carbon contains the increased quinone amount, where redox reactions with protons occur, resulting in an improved capacitance of 219 F g^{-1} in 1 M H_2SO_4, 2.6 times higher than that of PVDC resin derived microporous carbon (P-750 sample). On the contrary, the carboxylic acid groups, which react with hydroxide ions, were reduced in the prepared carbon. Accordingly, in the alkaline 6 M KOH, the specific capacitance of P-1ZnO-950 relatively increased modestly to 201 F g^{-1} compared to 178 F g^{-1} of P-750. Nonetheless, the highest rate capability of 79% was achieved based on the free access of the small ions in KOH solution onto the expanded pores. In summary, we devised a simple route for the synthesis of porous carbon using PVDC resin precursor by the dual role of ZnO agent with a low chemical ratio. The presence of functional groups in the synthesized activated carbon resulted in high specific capacitance of the carbon samples in acidic electrolyte and high rate capabilities in alkaline electrolyte.

CRediT authorship contribution statement

Beodl Hwang: Conceptualization, Methodology, Validation, Formal analysis, Investigation, Data curation, Writing - original draft, Visualization. **Seong-Hoon Yi:** Writing - review & editing. **Sang-Eun Chun:** Conceptualization, Methodology, Validation, Formal analysis, Data curation, Writing - review & editing, Visualization, Supervision, Funding acquisition.

Declaration of Competing Interest

The authors declare that they have no known competing financial interests or personal relationships that could have appeared to influence the work reported in this paper.

Acknowledgements

This work was supported by the National Research Foundation of Korea (NRF) grant funded by the Korean government (Ministry of Science, ICT & Future Planning) (NRF-2020R1F1A1075601) (NRF-2021R1A4A2001658).

References

[1] H. Marsh, F.R. Reinoso, Activated Carbon, Elsevier Science, 2006.
[2] T.J. Bandosz, J. Jagie-l-lo, K. Putyera, J.A. Schwarz, Sieving properties of carbons obtained by template carbonization of polyfurfuryl alcohol within mineral matrixes, Langmuir 11 (1995) 3964–3969.

[3] E. Frackowiak, F. Beguin, Carbon materials for the electrochemical storage of energy in capacitors, Carbon 39 (2001) 937–950.
[4] A. Borenstein, O. Hanna, R. Attias, S. Luski, T. Brousse, D. Aurbach, Carbon-based composite materials for supercapacitor electrodes: A review, J. Mater. Chem. A 5 (2017) 12653–12672.
[5] S. Dutta, A. Bhaumik, K.-C.-W. Wu, Hierarchically porous carbon derived from polymers and biomass: Effect of interconnected pores on energy applications, Energy Environ. Sci. 7 (2014) 3574–3592.
[6] Y. Wang, P. Niu, J. Li, S. Wang, L. Li, Recent progress of phosphorus composite anodes for sodium/potassium ion batteries, Energy Storage Mater. 34 (2021) 436–460.
[7] P. Simon, Y. Gogotsi, Capacitive energy storage in nanostructured carbon–electrolyte systems, Acc. Chem. Res. 46 (2013) 1094–1103.
[8] L. Weinstein, R. Dash, Supercapacitor carbons, Mater. Today 10 (2013) 356–357.
[9] A.M. Abioye, F.N. Ani, Recent development in the production of activated carbon electrodes from agricultural waste biomass for supercapacitors: A review, Renew. Sustain. Energy Rev. 52 (2015) 1282–1293.
[10] O. Ioannidou, A. Zabaniotou, Agricultural residues as precursors for activated carbon production—A review, Renew. Sustain. Energy Rev. 11 (2007) 1966–2005.
[11] J. Maciá-Agulló, B. Moore, D. Cazorla-Amorós, A. Linares-Solano, Activation of coal tar pitch carbon fibres: Physical activation vs. chemical activation, Carbon 42 (2004) 1367–1370.
[12] A. Ahmadpour, D. Do, The preparation of active carbons from coal by chemical and physical activation, Carbon 34 (1996) 471–479.
[13] T. Zhang, W.P. Walawender, L. Fan, M. Fan, D. Daugaard, R. Brown, Preparation of activated carbon from forest and agricultural residues through CO_2 activation, Chem. Eng. J. 105 (2004) 53–59.
[14] M. Ruiz-Fernández, M. Alexandre-Franco, C. Fernández-González, V. Gómez-Serrano, Development of activated carbon from vine shoots by physical and chemical activation methods, some insight into activation mechanism, Adsorption 17 (2011) 621–629.
[15] H. Teng, S.-C. Wang, Preparation of porous carbons from phenol–formaldehyde resins with chemical and physical activation, Carbon 38 (2000) 817–824.
[16] W. Shen, Z. Li, Y. Liu, Surface chemical functional groups modification of porous carbon, Recent Pat. Chem. Eng. 1 (2008) 27–40.
[17] J. Bedia, M. Peñas-Garzón, A. Gómez-Avilés, J.J. Rodriguez, C. Belver, Review on activated carbons by chemical activation with $FeCl_3$–C, J Carbon Res. 6 (2020) 21.
[18] M. Danish, R. Hashim, M.M. Ibrahim, O. Sulaiman, Effect of acidic activating agents on surface area and surface functional groups of activated carbons produced from *Acacia mangium* wood, J. Anal. Appl. Pyrol. 104 (2013) 418–425.
[19] S.L. Candelaria, B.B. Garcia, D. Liu, G. Cao, Nitrogen modification of highly porous carbon for improved supercapacitor performance, J. Mater. Chem. 22 (2012) 9884–9889.
[20] M. Lillo-Ródenas, D. Cazorla-Amorós, A. Linares-Solano, Understanding chemical reactions between carbons and NaOH and KOH: An insight into the chemical activation mechanism, Carbon 41 (2003) 267–275.
[21] C.-H. Yang, Q.D. Nguyen, T.-H. Chen, A.S. Helal, J. Li, J.-K. Chang, Functional group-dependent supercapacitive and aging properties of activated carbon electrodes in organic electrolyte, ACS Sustainable Chem. Eng. 6 (2018) 1208–1214.
[22] X. Lin, Y. Liang, Z. Lu, H. Lou, X. Zhang, S. Liu, B. Zheng, R. Liu, R. Fu, D. Wu, Mechanochemistry: A green, activation-free and top-down strategy to high-surface-area carbon materials, ACS Sustainable Chem. Eng. 5 (2017) 8535–8540.
[23] H.-Q. Li, R.-L. Liu, D.-Y. Zhao, Y.-Y. Xia, Electrochemical properties of an ordered mesoporous carbon prepared by direct tri-constituent co-assembly, Carbon 45 (2007) 2628–2635.
[24] J.-G. Wang, H. Liu, H. Sun, W. Hua, H. Wang, X. Liu, B. Wei, One-pot synthesis of nitrogen-doped ordered mesoporous carbon spheres for high-rate and long-cycle life supercapacitors, Carbon 127 (2018) 85–92.
[25] Y. Zhu, S. Murali, M.D. Stoller, K. Ganesh, W. Cai, P.J. Ferreira, A. Pirkle, R. M. Wallace, K.A. Cychosz, M. Thommes, Carbon-based supercapacitors produced by activation of graphene, Science 332 (2011) 1537–1541.
[26] X. Chen, R. Paul, L. Dai, Carbon-based supercapacitors for efficient energy storage, Natl. Sci. Rev. 4 (2017) 453–489.
[27] J.W. Jeon, L. Zhang, J.L. Lutkenhaus, D.D. Laskar, J.P. Lemmon, D. Choi, M. I. Nandasiri, A. Hashmi, J. Xu, R.K. Motkuri, Controlling porosity in lignin-derived nanoporous carbon for supercapacitor applications, ChemSusChem 8 (2015) 428–432.
[28] N. Blomquist, T. Wells, B. Andres, J. Bäckström, S. Forsberg, H. Olin, Metal-free supercapacitor with aqueous electrolyte and low-cost carbon materials, Sci. Rep. 7 (2017) 39836.
[29] I.-S. Son, Y. Oh, S.-H. Yi, W.B. Im, S.-E. Chun, Facile fabrication of mesoporous carbon from mixed polymer precursor of PVDF and PTFE for high-power supercapacitors, Carbon 159 (2020) 283–291.
[30] Q. Ma, H. Xie, J. Qu, Z. Zhao, B. Zhang, Q. Song, P. Xing, H. Yin, Tailoring the polymer-derived carbon encapsulated silicon nanoparticles for high-performance lithium-ion battery anodes, ACS Appl. Energy Mater. 3 (2019) 268–278.
[31] H. Zhu, X. Wang, X. Liu, X. Yang, Integrated synthesis of poly (o-phenylenediamine)-derived carbon materials for high performance supercapacitors, Adv. Mater. 24 (2012) 6524–6529.
[32] T. Zhu, J. Zhou, Z. Li, S. Li, W. Si, S. Zhuo, Hierarchical porous and N-doped carbon nanotubes derived from polyaniline for electrode materials in supercapacitors, J. Mater. Chem. A 2 (2014).
[33] M. Yang, X. Long, H. Li, H. Chen, P. Liu, Porous organic-polymer-derived nitrogen-doped porous carbon nanoparticles for efficient oxygen reduction electrocatalysis and supercapacitors, ACS Sustainable Chem. Eng. 7 (2018) 2236–2244.
[34] M. Wang, J. Yang, S. Liu, M. Li, C. Hu, J. Qiu, Nitrogen-doped hierarchically porous carbon nanosheets derived from polymer/graphene oxide hydrogels for high-performance supercapacitors, J. Colloid Interface Sci. 560 (2020) 69–76.
[35] B. Xu, F. Wu, S. Chen, G. Cao, Z. Zhou, A simple method for preparing porous carbon by PVDC pyrolysis, Colloids Surf. A 316 (2008) 85–88.
[36] M. Endo, Y. Kim, T. Takeda, T. Maeda, T. Hayashi, K. Koshiba, H. Hara, M. Dresselhaus, Poly (vinylidene chloride)-based carbon as an electrode material for high power capacitors with an aqueous electrolyte, J. Electrochem. Soc. 148 (2001) A1135.
[37] R. Bohme, R. Wessling, The thermal decomposition of poly (vinylidene chloride) in the solid state, J. Appl. Polym. Sci. 16 (1972) 1761–1778.
[38] M. Endo, Y. Kim, K. Ishii, T. Inoue, T. Takeda, T. Maeda, T. Nomura, N. Miyashita, M. Dresselhaus, Structure and application of various Saran-based carbons to aqueous electric double-layer capacitors, J. Electrochem. Soc. 149 (2002) A1473.
[39] M. Endo, Y. Kim, K. Ishii, T. Inoue, T. Nomura, N. Miyashita, M. Dresselhaus, Heat-treatment retention time dependence of polyvinylidenechloride-based carbons on their application to electric double-layer capacitors, J. Mater. Res. 18 (2003) 693–701.
[40] P.R. Roberge, R. Beaudoin, J.-F. Berthiaume, Fabrication and characterization of an activated carbon for electrochemical applications, Carbon 26 (1988) 173–182.
[41] B. Xu, F. Wu, S. Chen, Z. Zhou, G. Cao, Y. Yang, High-capacitance carbon electrode prepared by PVDC carbonization for aqueous EDLCs, Electrochim. Acta 54 (2009) 2185–2189.
[42] P. Strubel, S. Thieme, T. Biemelt, A. Helmer, M. Oschatz, J. Brückner, H. Althues, S. Kaskel, ZnO hard templating for synthesis of hierarchical porous carbons with tailored porosity and high performance in lithium-sulfur battery, Adv. Funct. Mater. 25 (2015) 287–297.
[43] Q. Wang, J. Yan, Y. Wang, T. Wei, M. Zhang, X. Jing, Z. Fan, Three-dimensional flower-like and hierarchical porous carbon materials as high-rate performance electrodes for supercapacitors, Carbon 67 (2014) 119–127.
[44] G.W. Liu, T.Y. Chen, C.H. Chung, H.P. Lin, C.H. Hsu, Hierarchical micro/mesoporous carbons synthesized with a ZnO template and petroleum pitch via a solvent-free process for a high-performance supercapacitor, ACS Omega 2 (2017) 2106–2113.
[45] X. He, X. Li, H. Ma, J. Han, H. Zhang, C. Yu, N. Xiao, J. Qiu, ZnO template strategy for the synthesis of 3D interconnected graphene nanocapsules from coal tar pitch as supercapacitor electrode materials, J. Power Sources 340 (2017) 183–191.
[46] M. Sarker, M.M. Rashid, Polyvinyl chloride (PVC) waste plastic treatment using zinc oxide (ZnO) with activated carbon and produced hydrocarbon fuel for petroleum refinery, Int. Eng. Sci 1 (2012) 29–41.
[47] F. Caturla, M. Molina-Sabio, F. Rodriguez-Reinoso, Preparation of activated carbon by chemical activation with $ZnCl_2$, Carbon 29 (1991) 999–1007.
[48] M. Olivares-Marín, C. Fernández-González, A. Macías-García, V. Gómez-Serrano, Preparation of activated carbon from cherry stones by chemical activation with $ZnCl_2$, Appl. Surf. Sci. 252 (2006) 5967–5971.
[49] J. Gamby, P. Taberna, P. Simon, J. Fauvarque, M. Chesneau, Studies and characterisations of various activated carbons used for carbon/carbon supercapacitors, J. Power Sources 101 (2001) 109–116.
[50] A. González, E. Goikolea, J.A. Barrena, R. Mysyk, Review on supercapacitors: Technologies and materials, Renew. Sustain. Energy Rev. 58 (2016) 1189–1206.
[51] J. Jiang, H. Chen, Z. Wang, L. Bao, Y. Qiang, S. Guan, J. Chen, Nitrogen-doped hierarchical porous carbon microsphere through KOH activation for supercapacitors, J. Colloid Interface Sci. 452 (2015) 54–61.
[52] L. Wei, G. Yushin, Electrical double layer capacitors with activated sucrose-derived carbon electrodes, Carbon 49 (2011) 4830–4838.
[53] L. Sun, C. Wang, Y. Zhou, Q. Zhao, X. Zhang, J. Qiu, Activated nitrogen-doped carbons from polyvinyl chloride for high-performance electrochemical capacitors, J. Solid State Electrochem. 18 (2014) 49–58.
[54] S.-E. Chun, J. Whitacre, Formation of micro/mesopores during chemical activation in tailor-made nongraphitic carbons, Microporous Mesoporous Mater. 251 (2017) 34–41.
[55] D. Zhu, Y. Wang, L. Gan, M. Liu, K. Cheng, Y. Zhao, X. Deng, D. Sun, Nitrogen-containing carbon microspheres for supercapacitor electrodes, Electrochim. Acta 158 (2015) 166–174.
[56] J. Wang, P. Nie, B. Ding, S. Dong, X. Hao, H. Dou, X. Zhang, Biomass derived carbon for energy storage devices, J. Mater. Chem. A 5 (2017) 2411–2428.
[57] C. Long, L. Jiang, X. Wu, Y. Jiang, D. Yang, C. Wang, T. Wei, Z. Fan, Facile synthesis of functionalized porous carbon with three-dimensional interconnected pore structure for high volumetric performance supercapacitors, Carbon 93 (2015) 412–420.
[58] S. Altenor, B. Carene, E. Emmanuel, J. Lambert, J.J. Ehrhardt, S. Gaspard, Adsorption studies of methylene blue and phenol onto vetiver roots activated carbon prepared by chemical activation, J. Hazard Mater. 165 (2009) 1029–1039.
[59] Y.-H. Lee, K.-H. Chang, C.-C. Hu, Differentiate the pseudocapacitance and double-layer capacitance contributions for nitrogen-doped reduced graphene oxide in acidic and alkaline electrolytes, J. Power Sources 227 (2013) 300–308.
[60] B. Xu, S. Hou, M. Chu, G. Cao, Y. Yang, An activation-free method for preparing microporous carbon by the pyrolysis of poly (vinylidene fluoride), Carbon 48 (2010) 2812–2814.

[61] J. Donald, Y. Ohtsuka, C.C. Xu, Effects of activation agents and intrinsic minerals on pore development in activated carbons derived from a Canadian peat, Mater. Lett. 65 (2011) 744–747.
[62] Z. Yue, C.L. Mangun, J. Economy, Preparation of fibrous porous materials by chemical activation: 1. $ZnCl_2$ activation of polymer-coated fibers, Carbon 40 (2002) 1181–1191.
[63] J. Zhang, W. Zhang, M. Han, J. Pang, One pot synthesis of nitrogen-doped hierarchical porous carbon derived from phenolic formaldehyde resin with sodium citrate as activation agent for supercapacitors, J. Mater. Sci.: Mater. Electron. 29 (2018) 4639–4648.
[64] H. Teng, T.-S. Yeh, Preparation of activated carbons from bituminous coals with zinc chloride activation, Ind. Eng. Chem. Res. 37 (1998) 58–65.
[65] G. Zhang, H. Luo, H. Li, L. Wang, B. Han, H. Zhang, Y. Li, Z. Chang, Y. Kuang, X. Sun, ZnO-promoted dechlorination for hierarchically nanoporous carbon as superior oxygen reduction electrocatalyst, Nano Energy 26 (2016) 241–247.
[66] T.-H. Liou, Development of mesoporous structure and high adsorption capacity of biomass-based activated carbon by phosphoric acid and zinc chloride activation, Chem. Eng. J. 158 (2010) 129–142.
[67] D.V. Lam, K. Jo, C.H. Kim, J.H. Kim, H.J. Lee, S.M. Lee, Activated carbon textile via chemistry of metal extraction for supercapacitors, ACS Nano 10 (2016) 11351–11359.
[68] L. Wang, Q. Zhu, J. Zhao, Y. Guan, J. Liu, Z. An, B. Xu, Nitrogen-doped hierarchical porous carbon for supercapacitors with high rate performance, Microporous Mesoporous Mater. 279 (2019) 439–445.
[69] A. Berman, M. Epstein, The kinetic model for carboreduction of zinc oxide, Le, J. Phys. IV 9 (1999) Pr3-319–Pr313-324.
[70] H. Wang, S. Yu, B. Xu, Hierarchical porous carbon materials prepared using nano-ZnO as a template and activation agent for ultrahigh power supercapacitors, Chem. Commun. 52 (2016) 11512–11515.
[71] C. Wang, T. Liu, Nori-based N, O, S, Cl co-doped carbon materials by chemical activation of $ZnCl_2$ for supercapacitor, J. Alloy. Compd. 696 (2017) 42–50.
[72] Y. Huang, Z. Liu, G. Zhao, Reaction process for $ZnCl_2$ activation of phenol liquefied wood fibers, RSC Adv. 6 (2016) 78909–78917.
[73] X. Song, Q. Chen, E. Shen, H. Liu, N-Doped 3D hierarchical carbon from resorcinol–formaldehyde–melamine resin for high-performance supercapacitors, New J. Chem. 44 (2020) 8638–8649.
[74] J. Chen, H. Wei, H. Chen, W. Yao, H. Lin, S. Han, N/P co-doped hierarchical porous carbon materials for superior performance supercapacitors, Electrochim. Acta 271 (2018) 49–57.
[75] K. Xia, Q. Gao, J. Jiang, J. Hu, Hierarchical porous carbons with controlled micropores and mesopores for supercapacitor electrode materials, Carbon 46 (2008) 1718–1726.
[76] E. Altintig, S. Kirkil, Preparation and properties of Ag-coated activated carbon nanocomposites produced from wild chestnut shell by $ZnCl_2$ activation, J. Taiwan Inst. Chem. Eng. 63 (2016) 180–188.
[77] A. Elmouwahidi, E. Bailón-García, A.F. Pérez-Cadenas, F.J. Maldonado-Hódar, F. Carrasco-Marín, Activated carbons from KOH and H_3PO_4-activation of olive residues and its application as supercapacitor electrodes, Electrochim. Acta 229 (2017) 219–228.
[78] B. Wang, J. Qiu, H. Feng, E. Sakai, T. Komiyama, KOH-activated nitrogen doped porous carbon nanowires with superior performance in supercapacitors, Electrochim. Acta 190 (2016) 229–239.
[79] S.-E. Chun, J. Choi, J.F. Whitacre, Tailoring the porous texture of activated carbons by CO_2 reactivation to produce electrodes for organic electrolyte-based EDLCs, Ionics 24 (2018) 2055–2061.
[80] K. Babel, K. Jurewicz, KOH activated carbon fabrics as supercapacitor material, J. Phys. Chem. Solids 65 (2004) 275–280.
[81] C. Huang, T. Sun, D. Hulicova-Jurcakova, Wide electrochemical window of supercapacitors from coffee bean-derived phosphorus-rich carbons, ChemSusChem 6 (2013) 2330–2339.
[82] M. Chen, X. Kang, T. Wumaier, J. Dou, B. Gao, Y. Han, G. Xu, Z. Liu, L. Zhang, Preparation of activated carbon from cotton stalk and its application in supercapacitor, J. Solid State Electrochem. 17 (2012) 1005–1012.
[83] Z. Zou, J. Zhao, J. Xue, R. Huang, C. Jiang, Highly porous carbon spheres prepared by boron-templating and reactive H_3PO_4 activation as electrode of supercapacitors, J. Electroanal. Chem. 799 (2017) 187–193.
[84] S. Ahmed, A. Ahmed, M. Rafat, Supercapacitor performance of activated carbon derived from rotten carrot in aqueous, organic and ionic liquid based electrolytes, J. Saudi Chem. Soc. 22 (2018) 993–1002.
[85] X. He, P. Ling, M. Yu, X. Wang, X. Zhang, M. Zheng, Rice husk-derived porous carbons with high capacitance by $ZnCl_2$ activation for supercapacitors, Electrochim. Acta 105 (2013) 635–641.
[86] J. Zhang, L. Gong, K. Sun, J. Jiang, X. Zhang, Preparation of activated carbon from waste *Camellia oleifera* shell for supercapacitor application, J. Solid State Electrochem. 16 (2012) 2179–2186.
[87] A. Wollbrink, K. Volgmann, J. Koch, K. Kanthasamy, C. Tegenkamp, Y. Li, H. Richter, S. Kämnitz, F. Steinbach, A. Feldhoff, Amorphous, turbostratic and crystalline carbon membranes with hydrogen selectivity, Carbon 106 (2016) 93–105.
[88] Y. Liu, J.S. Xue, T. Zheng, J.R. Dahn, Mechanism of lithium insertion in hard carbons prepared by pyrolysis of epoxy resins, Carbon 34 (1996) 193–200.
[89] M.R. Jisha, Y.J. Hwang, J.S. Shin, K.S. Nahm, T. Prem Kumar, K. Karthikeyan, N. Dhanikaivelu, D. Kalpana, N.G. Renganathan, A.M. Stephan, Electrochemical characterization of supercapacitors based on carbons derived from coffee shells, Mater. Chem. Phys. 115 (2009) 33–39.
[90] S. Yorgun, N. Vural, H. Demiral, Preparation of high-surface area activated carbons from Paulownia wood by $ZnCl_2$ activation, Microporous Mesoporous Mater. 122 (2009) 189–194.
[91] E. Köseoğlu, C. Akmil-Başar, Preparation, structural evaluation and adsorptive properties of activated carbon from agricultural waste biomass, Adv. Powder Technol. 26 (2015) 811–818.
[92] M. Li, H. Xiao, T. Zhang, Q. Li, Y. Zhao, Activated carbon fiber derived from sisal with large specific surface area for high-performance supercapacitors, ACS Sustainable Chem. Eng. 7 (2019) 4716–4723.
[93] G.S. Foo, C. Sievers, Synergistic effect between defect sites and functional groups on the hydrolysis of cellulose over activated carbon, ChemSusChem 8 (2015) 534–543.
[94] J. Tan, H. Chen, Y. Gao, H. Li, Nitrogen-doped porous carbon derived from citric acid and urea with outstanding supercapacitance performance, Electrochim. Acta 178 (2015) 144–152.
[95] Y. Wang, J. Chen, J. Cao, Y. Liu, Y. Zhou, J.-H. Ouyang, D. Jia, Graphene/carbon black hybrid film for flexible and high rate performance supercapacitor, J. Power Sources 271 (2014) 269–277.
[96] H. Wang, R. Fan, J. Miao, J. Deng, Y. Wang, Oxygen groups immobilized on micropores for enhancing the pseudocapacitance, ACS Sustainable Chem. Eng. 7 (2019) 11407–11414.
[97] Z. Liu, Z. Zhao, Y. Wang, S. Dou, D. Yan, D. Liu, Z. Xia, S. Wang, In situ exfoliated, edge-rich, oxygen-functionalized graphene from carbon fibers for oxygen electrocatalysis, Adv. Mater. 29 (2017) 1606207.
[98] X. Chen, J. Zhang, B. Zhang, S. Dong, X. Guo, X. Mu, B. Fei, A novel hierarchical porous nitrogen-doped carbon derived from bamboo shoot for high performance supercapacitor, Sci. Rep. 7 (2017) 1–11.
[99] B. Li, F. Dai, Q. Xiao, L. Yang, J. Shen, C. Zhang, M. Cai, Nitrogen-doped activated carbon for a high energy hybrid supercapacitor, Energy Environ. Sci. 9 (2016) 102–106.
[100] M.S. Shafeeyan, W.M.A.W. Daud, A. Houshmand, A. Shamiri, A review on surface modification of activated carbon for carbon dioxide adsorption, J. Anal. Appl. Pyrol. 89 (2010) 143–151.
[101] X.-R. Li, Y.-H. Jiang, P.-Z. Wang, Y. Mo, W.-D. Lai, Z.-J. Li, R.-J. Yu, Y.-T. Du, X.-R. Zhang, Y. Chen, Effect of the oxygen functional groups of activated carbon on its electrochemical performance for supercapacitors, New Carbon Mater. 35 (2020) 232–243.
[102] D. Hulicova-Jurcakova, M. Seredych, G.Q. Lu, T.J. Bandosz, Combined effect of nitrogen-and oxygen-containing functional groups of microporous activated carbon on its electrochemical performance in supercapacitors, Adv. Funct. Mater. 19 (2009) 438–447.
[103] N. Subramanian, B. Viswanathan, Nitrogen-and oxygen-containing activated carbons from sucrose for electrochemical supercapacitor applications, RSC Adv. 5 (2015) 63000–63011.
[104] G. Sun, D. Long, X. Liu, W. Qiao, L. Zhan, X. Liang, L. Ling, Asymmetric capacitance response from the chemical characteristics of activated carbons in KOH electrolyte, J. Electroanal. Chem. 659 (2011) 161–167.
[105] V. Barranco, M. Lillo-Rodenas, A. Linares-Solano, A. Oya, F. Pico, J. Ibañez, F. Agullo-Rueda, J.M. Amarilla, J. Rojo, Amorphous carbon nanofibers and their activated carbon nanofibers as supercapacitor electrodes, J. Phys. Chem. C 114 (2010) 10302–10307.
[106] J.-W. Lang, X.-B. Yan, W.-W. Liu, R.-T. Wang, Q.-J. Xue, Influence of nitric acid modification of ordered mesoporous carbon materials on their capacitive performances in different aqueous electrolytes, J. Power Sources 204 (2012) 220–229.